

Polarization evolution dynamics of dissipative soliton fiber laser

LEI GAO^{1,*}, YULONG CAO¹, YUJIA LI¹, STEFAN WABNITZ^{2,3}, WEI HUANG¹,
HONGQING RAN¹, DANQI FENG¹, LIGANG HUANG¹, XIAOSHENG TANG¹, AND TAO
ZHU^{1,*}

1 Key Laboratory of Optoelectronic Technology & Systems (Ministry of Education), Chongqing University, Chongqing, 400044, China.

2 Dipartimento di Ingegneria dell'Informazione, Università degli Studi di Brescia and INO-CNR, via Branze 38, 25123 Brescia, Italy.

3 Novosibirsk State University, 1 Pirogova str, Novosibirsk 630090, Russia.

*Corresponding authors: gaolei@cqu.edu.cn; zhutao@cqu.edu.cn

Dissipative solitons are localized solutions in non-integrable and non-conservative nonlinear system, due to a balance of nonlinearity, dispersion, filtering, and loss/gain. Different from conventional soliton, they exhibit extremely complex and striking dynamics, and are more universal in the far-from-equilibrium natural system. Taking advantage of dispersive Fourier transform and time lens, the spatio-temporal transient dynamics of dissipative solitons have been characterized with both amplitude and phase. Yet, a full avenue of the buildup process of dissipative soliton is full of debris for the lack of the polarization evolution information. Here, we characterize the probabilistic polarization distributions in the buildup of dissipative soliton in a net-normal dispersion fiber laser system mode-locked by single-wall carbon nanotubes. The lasing system operates from random amplified spontaneous emission to stable dissipative soliton when the cavity gain is increasing, and state of polarization of each wavelength convergence exponentially towards a fixed point. To reveal the invariant polarization relationship among various wavelengths, the phase diagram of the ellipticity angle and spherical orientation angle is introduced. We find that the polarization of each filtered wavelength in the central region of the dissipative soliton is linearly spaced, while those in the two fronts are spatially varying. Increasing cavity gain leads to spectrum broadening, meanwhile, the polarizations of the new generated frequencies are extending to scatter. Further increasing pump power results into dissipative soliton explosion, during which a kind of polarization optical rogue waves is identified. Those experimental results provide more information for deeper insights into the transient dynamics of dissipative soliton fiber laser.

1. INTRODUCTION

Solitons are localized structures with specific analytical solutions in conservative and integrable systems, where the interaction of nonlinearity and diffraction/dispersion are balanced [1]. In optics, the conventional soliton systems possess a high degree of coherence, due to the well-defined phases among various longitudinal modes. They propagate with transformed-limited pulse duration, and collide with each other while maintaining their shapes and velocities. Yet, the natural system always to be dissipative and nonintegrable, and various localized structures, such as the Akhmediev breathers, quasisoliton, and dissipative solitons, or even sporadic rogue waves, proliferate and decay with diverse spatial-temporal periodic and localized structures [2-4].

Dissipative solitons (DSs) are high coherent solutions due to a balance of nonlinearity, dispersion, filtering, and loss/gain [1-4]. Different from conventional soliton in integrable fiber laser system with anomalous dispersion, the DSs in dissipative fiber laser system with normal dispersion exhibit extremely complex and striking dynamics. For example, the much broader pulse duration and linear phase chirping make them ideal for high energy ultrafast fiber laser and phase-dependent optical processing, and the flat and broad optical spectrum provides an excellent platform for high coherent laser source. Extensive theoretical analysis on the DS in mode-locked fiber laser system have been performed [5], while direct experiments on its buildup dynamics are restricted by the relative slow detecting techniques. Based on the well-developed dispersive Fourier transform (DFT), the non-repetitive optical signals are transformed into temporal data under far-field

approximation, and the spectral properties of soliton, soliton explosion, soliton molecules, modulation instability, and supercontinuum are characterized [6-14]. Similarly, the time lens that utilize temporal analogue of spatial lens have been taken for characterization of the real-time pulse temporal properties of transient DS [15,16]. However, the confidence of the amplitude and phase in spatio-temporal transient dynamics is relying on the assumption of the strict correspondence between the temporal and spectral domains. This assumption is suspicious in the transient optical dynamics, where the phases may be loosely locked, or even irrelevant. This is especially important in the proliferating period of the DS, where, for example, the state of polarization (SOP) of any longitudinal modes in any time may be indeterministic [17-22]. This incompleteness makes a full avenue of the buildup dynamics of DS full of debris.

In this letter, we experimentally investigate the probabilistic nature of SOP distribution in the buildup dynamics of DS. It proliferates from the random noise in a fiber ring laser cavity with net normal dispersion, which is mode-locked by a saturable absorber (SA) made from single-wall carbon nanotubes. We characterize the probabilistic SOP distribution by introducing the phase diagram of the ellipticity angle χ and spherical orientation angle ψ . We find the inversely exponential tendency of the SOP with increasing cavity gain, and the spatially varying structure along their spectral components of a stable DS. A kind of polarization optical rogue waves is also identified when the high coherence is deteriorated by a higher cavity gain.

2. MAIN PRINCIPLE AND SETUP

Figure 1 schematically depicts the ring fiber cavity containing 15 m erbium-doped fiber (EDF, Nufern, EDFC-980-HP) forward pumped by a 976 nm continuous wave laser through wavelength division multiplexer (WDM), a polarization independent optical isolator (ISO), a polarization controller (PC), 2.7 m single mode fiber (SMF), and an optical coupler (OC) with a 10% output port. The dispersion parameters of EDF and SMF are -12.2 and 18 ps/nm/km, respectively. Therefore, the total 17.8 m ring cavity possesses a net normal dispersion of 0.171 ps². The saturable absorbing film is made by mixing 10 wt% aqueous polyvinyl alcohol and 0.5 mg/mL single-wall-carbon-nanotubes solution at a volume ratio of 1:2, then dehydrated in vacuum [23]. Its nonlinear optical response is measured based on a home-made balanced two-detector methods as described in [24]. The modulation depth and the saturable power are 3.5% and 30.73 MW/cm², respectively [23]. This low saturable power renders the laser system operating at DS with relative low pump power, while also made the DS unstable for larger gain due to the bleaching effect of the SA.

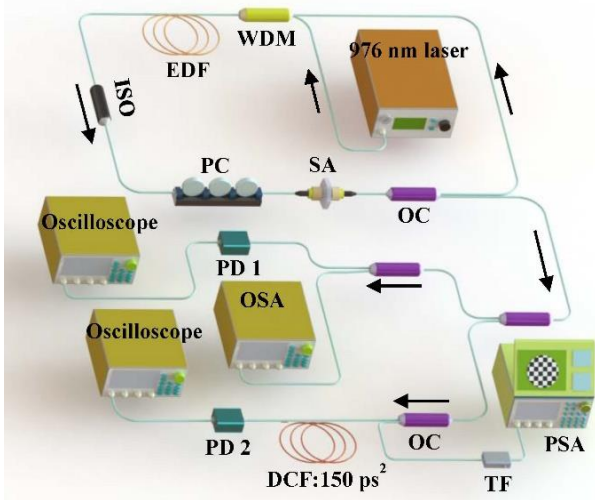


Fig. 1. Schematic of the ring fiber laser cavity and measurement methods.

The output characterized is detected by an optical spectrum analyzer (OSA, Yokogawa, AQ6370), an autocorrelator (APE, Pulse check), an oscilloscope (Lecroy, SDA 8600A), and a frequency analyzer (Agilent, PSA E4447A), together with a photodetector (PD1) with a bandwidth of 350 MHz. The state of polarization (SOP) of the DS is measured by a high speed polarization state analyzer (PSA, General Photonics, PSGA-101-A) after filtered by a tunable optical filter (TF, Santec, OTF-320) with a bandwidth of 0.2 nm. Meanwhile, we also detect their single-shot spectra based on a home-made DFT, where periodic signals are stretched by 500 m dispersion compensation fiber (DCF) with a dispersion of 150 ps² for frequency-to-time transformation, and subsequently fed to a 50 GHz PD2 connected to a real time oscilloscope (Tektronix, DPO 71254) with bandwidth of 12.5 GHz.

3. RESULTS AND DISCUSSION

For this configuration, stable DS can be observed for pump power larger than 55 mW with easiness. The typical output parameters for pump power at 55 mW are depicted in Fig. 2, where rectangle-shaped optical spectrum with a full width at half maximum (FWHM) of 13.6 nm is shown. The autocorrelation trace exhibits a FWHM duration of 30.5 ps, when fitted by a Gaussian function. The signal to noise ratio at the fundamental frequency of 11.48 MHz exceeds 70 dB. Specifically, we plot the optical spectra under various pump powers in Figs. 2(a)-(d). For pump power smaller than 55 mW, the laser system operates from random amplified spontaneous emission to quasi-DS regime, then it enters into stable DS. Further increasing cavity gain broaden the optical spectrum, while a much larger gain deteriorates the mode-locking state.

This deterioration can be deduced directly from the noisy new-emerged frequencies in the two fronts of DS optical spectrum in Fig. 2(d), of which shall originate from the stochastic longitudinal modes mixing under nonlinear optical response of the fabricated SA with low saturation power.

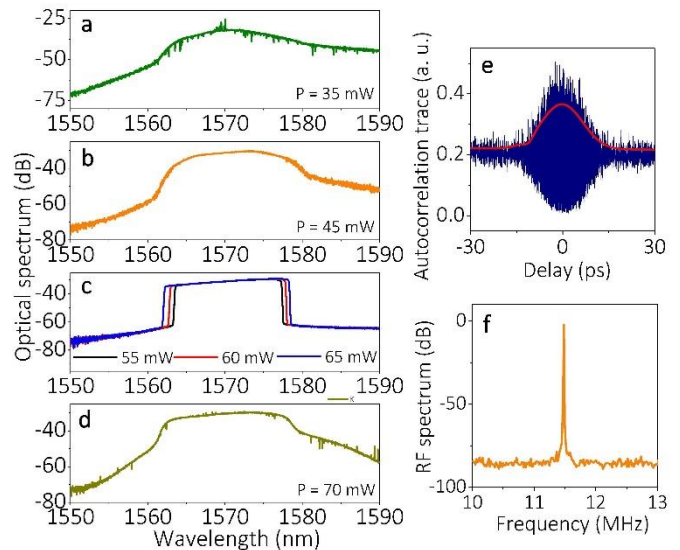


Fig. 2. Typical outputs for DS. (a)-(d) Averaged optical spectra for various pump powers. (e) Autocorrelation trace of pulses for pump power at 55 mW, which is fitted by Gauss function. (f) Radio frequency spectrum at the fundamental frequency of 11.48 MHz.

To further explore the intrinsic transient dynamics of the laser cavity, we give consecutive single-shot optical spectra in Fig. 3. Those real-time optical spectra corresponding to those in Figs. 2 (a), (b), (d) exhibit fine structures, which are invisible in the averaged optical spectrum. For example, Fig. 3 (a) says that a broad optical spectrum is formed for pump power at 35 mW. In fact, the laser system composes both the pulsed part, together with coupling continuous wave part, while the DFT can only reflect the pulsed part dynamics. We see that the optical spectrum grows based on the energy from the continuous wave part, and decays swiftly due to inefficient cavity gain, just similarly to the optical puff gestated in a partially mode-locked laser system [11,13]. Interestingly, it attends to generate new frequencies in the short wavelength side through wave mixing among bright stripes, while a giant center appears in the center wavelength region. Just following the formation of the maximum point, the whole broad spectrum collapses swiftly, and the energy returns to the continuous wave part, resulting into a zero-value mapping when detected by the DFT.

As a contrast, with the increment of cavity gain, the optical spectrum broadens gradually, and two giant peaks appear in the two fronts, of which can be shown in Fig. 3 (b) for pump power at 45 mW. Those two peaks assimilate the energies from the continuous wave part, and they continuously red-shift and blue-shift, respectively. Meantime, multiple mode mixing grows between the two peaks, which can be verified in Fig. 3 (e). After of the maximum value of those two peaks, the optical spectrum decays with a slower speed when compared with that of Fig. 3 (a). The pulsed part energy reflows into the continuous wave part.

The cavity gain here is still not sufficient to support stable DS, and the irregular clusters proliferate and decay, at various speeds in a memoryless manner, which only depends on the power in the cavity. Yet, great difference between the partially mode-locked laser and DS [13]. For example, we do not find the critical behavior in the buildup of DS. Typically, this behavior means that the proliferation time and decay time are the same, and it has been observed for the optical puff in forming turbulence. The reason is that their underlying physics are different: the evolution of the optical puff in partially mode-locked fiber laser system is only associated with the multiple-mode-mixing

[11,13], while the formation of optical cluster in a dissipative fiber laser system is more complex, involving both nonlinearity, dispersion, filtering, and loss/gain. In its decaying region, energy do not couple into

the center part gradually as for optical puff, but collapse swiftly into the continuous wave part.

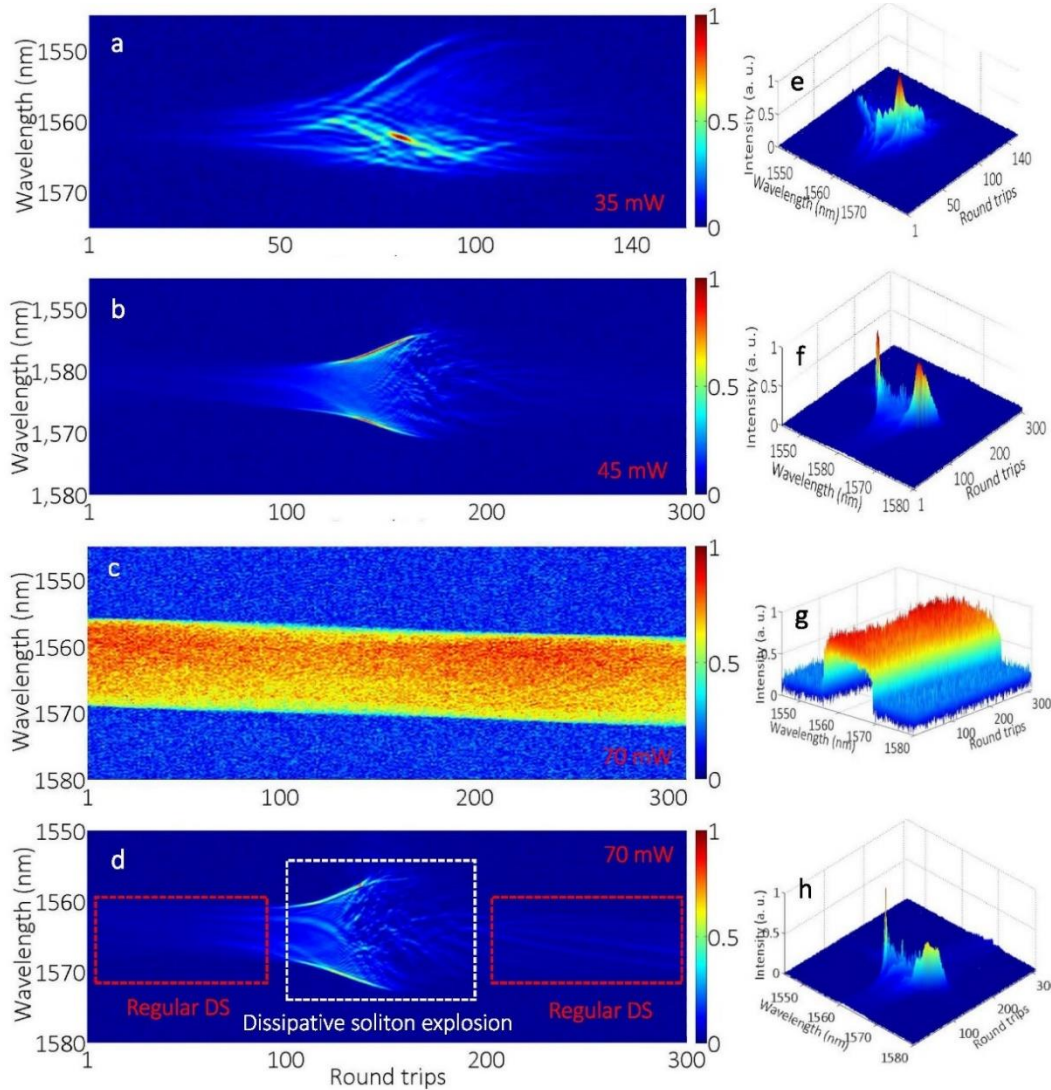


Fig. 3. Conservative single-shot spectra in the build-up of DS at various pump powers. (a)-(d), Pump power at 35 mW, 45 mW, and 70 mW, respectively. The corresponding 3D plots in (e)-(h) indicate giant peaks with rogue intensities in the spectral domain. Due to limited splicing error of long time series into pieces, a slight tilt is shown in the single-shot spectra. All the intensities are normalized with respect to the maximum value in each detection. The varying bright stripes intersect within conservative roundtrips, indicating intense multimode mixing.

For pump power between 55 mW and 65 mW, the DS operating stable. Yet, its average intensity during single-shot spectrum detection is much smaller than those of the unstable pulses as in Figs. 3(a), (b) and (d). Due to the large formation time, and the limited storage length of the real time oscilloscope, we do not detect the formation process of a stable DS. Yet, this information has been well known through single-shot detection based on DFT [4,8]. Instead, we care much about the deteriorated DS, usually induced by excessive cavity gain. This phenomenon has been frequently encountered when the saturable power of the SA is relative low, as just in our case with single-wall-carbon-nanotubes. As shown in Figs. 3 (c) and (g) for pump power at 70 mW, regular DS with neatly rectangle-shaped optical spectra are frequently detected, just as for pump power between 55 mW and 65 mW. Yet, a period of much broader optical spectra persisting near the square spectrum may also be occasionally encountered, and two

extremely high peaks are observed. One example is shown in Figs. 3 (d) and (h). After the spectral collapse, the DS returns its neat square shape with low much lower intensity. For this case, the whole transient evolution process takes within 50 roundtrips. Limited by the low dynamic ranges of the high speed PD2, the single-shot spectra of the stable DS is too low compared with the extremely high intensities during the transient stage. This phenomenon is referred as soliton explosions, where the balance of nonlinearity, dispersion, filtering and loss/gain for the DS is perturbed by the surplus cavity gain for larger pump power [25]. Part energy of the DS dissipates into continuous waves through such an explosion, and the DS maintains its high coherent pulse ensemble. Based thousands times of detections, we find that the probability for this giant peaks increases with the cavity gain, and the transient evolution will take more times to return the DS region.

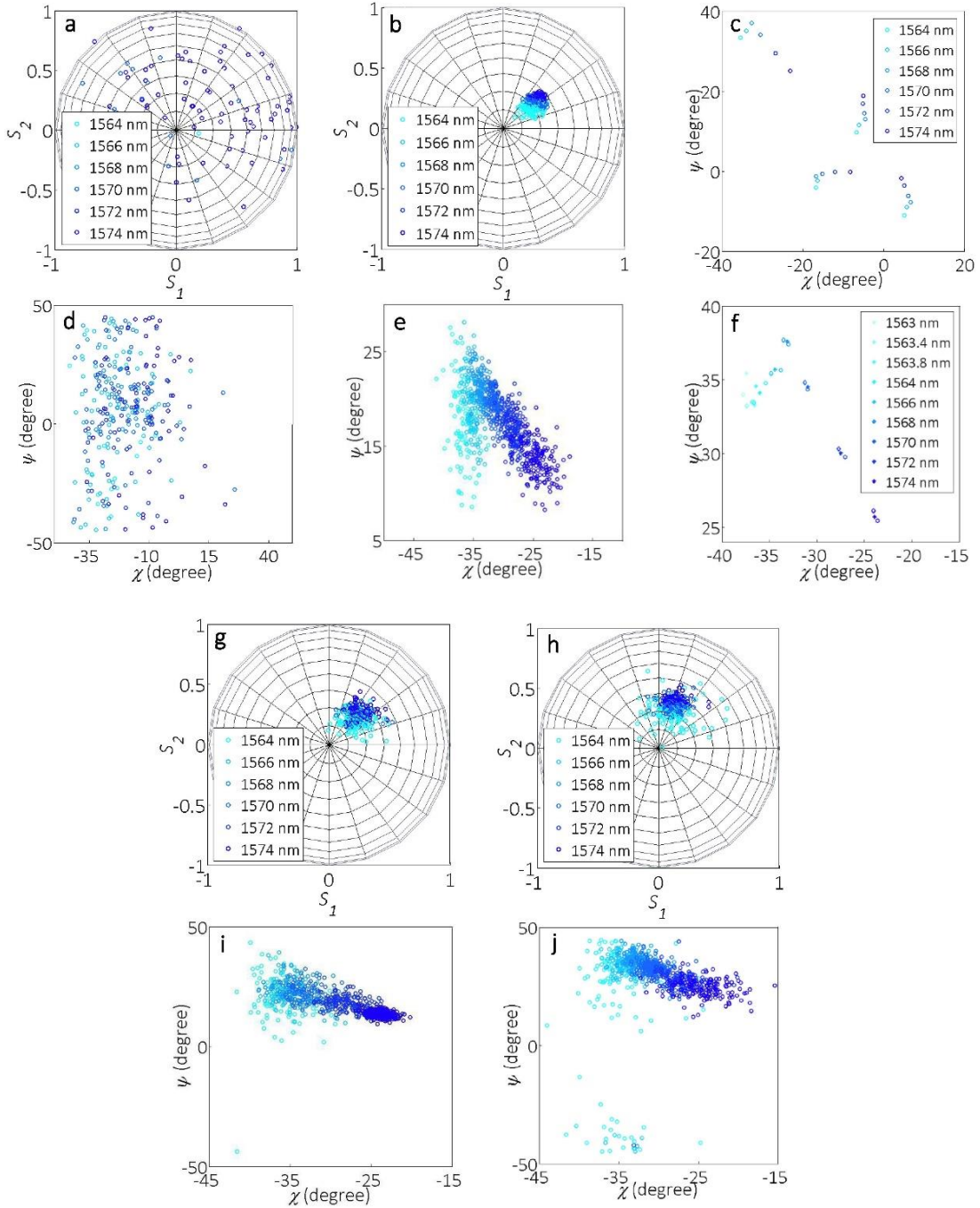


Fig. 4. States of polarization for various filtered wavelengths and different pump powers. (a), (b), (g), (h) Normalized Stokes parameters represented on the Poincaré sphere for pump powers at 35 mW, 45 mW, 67.5 mW, and 70 mW, respectively. The corresponding phase diagrams based on the ellipticity angle χ and spherical orientation angle ψ are shown in (d), (e), (i), (j). (c) Phase diagram for pump power at 55 mW, where the input absolute SOP is changed arbitrarily through biasing the fiber between output OC and the PSA, while the shape represented by χ and ψ is fixed. (f) Phase diagram for stable DSs, where pump power is 55 mW (circled dots), 60 mW (rectangle dots), 65 mW (pozidriv dots), respectively. The SOPs on the front exhibits fluctuations.

Those experimental data arose a question: why cannot the DS further broaden their spectrum indefinitely, when the pump power is increasing constantly, just like the case of dissipative soliton resonance [26]? To ascertain the question, we need to reconsider how the new frequencies are generated the DS from stochastic random to the well-known linear phase relationship. Although the single-shot spectra have been given, the exact SOP distributing characteristics of the lasing wavelengths will give more information for reconstructing the buildup process of DS. This information is especially important at the primary stage, where the DFT fails due to unfixed phase relationship. Therefore,

we measured the SOPs of each filtered wavelength of the dissipative fiber laser cavity with diverse pump powers. Figure 4 exhibit the SOP distributions for the cases in Fig. 2. It is clear from the points on the Poincaré sphere that the corresponding SOPs for each wavelength is evolving from random noise into a fixed point. This trend is more clear in the phase diagram of the ellipticity angle χ and spherical orientation angle ψ , which are calculated as following, respectively

$$\begin{cases} \chi = \frac{1}{2} \arctan\left(\frac{s_3}{\sqrt{s_1^2 + s_2^2}}\right) \\ \psi = \frac{1}{2} \arctan\left(\frac{s_2}{s_1}\right) \end{cases} \quad (1)$$

where, s_1, s_2, s_3 are the Stokes parameters of SOP. Different from the partially mode-locking [11], neither the bifurcation nor total turbulence is identified. As shown in Fig. 4 (d), the positions of the SOPs may be probabilistic for pump power at 35 mW, where the amplified spontaneous emission dominates. Yet, Fig. 4 (e) depicts that those for pump power at 45 mW all locate in the well-defined space in the phase diagram of χ and ψ , although still behave probabilistically.

Further increasing pump power leads to stable DS operation. As shown in Fig. 4 (c), a well-rectangle-shaped optical spectrum results into a fixed SOP distribution with a folding line. The distribution in the phase diagram of χ and ψ is invariant even the birefringence induced by the fiber between the output OC and the polarization state analyzer is changed. We observe a quasi-V shaped in Fig. 4 even the DS is not stable with insufficient cavity gain. One interesting finding is that the phase diagram for wavelengths in the central region of the DS is linearly spaced, while those in the blue side are spatially varying. The reason is the wavelength-dependence of the filtering film in the TF. Limited by the manufacturing process of the tunable filter, we can only tune the wavelength continuously from 1563 nm to 1574 nm, beyond which a sudden abrupt of the SOP for the longer wavelength is added. Yet, we observe a similar distribution in the phase diagram for wavelength larger than 1575 nm. That's to say, both fronts on the two directions feature spatially varying SOP distributions.

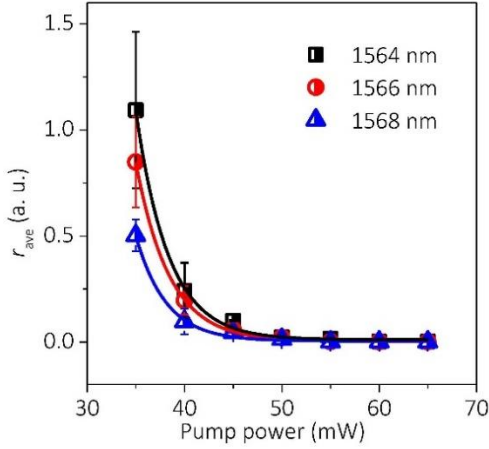


Fig. 5. The averaged relative distances for various wavelengths at different pump powers. An exponential convergence towards a fixed point is shown. Error bars represent absolute errors based on experimental data, which are relatively high for lower pump power.

As an intrinsic manner, a larger cavity gain will broaden the optical spectrum of stable DS through generating more new frequencies on the two fronts. This spectrum broadening has been verified by Fig. 2 (c), and its corresponding phase diagrams are depicted in Fig. 4 (f). We find that the new wavelengths on the two fronts feature irregular SOPs with positions more far away from the main distributions, and even those in the central region are shifted slightly. For example, when the pump power is 65 mW, the new frequencies on the fronts become unstable even the DS behave stable as a whole. Those experimental results hint the redistribution of the energy among lasing wavelengths when the cavity gain is changed. Nevertheless, such a phenomenon has hardly been taken for serious when building the theoretical model for dissipative mode-locked laser system. Besides, the spatially varying SOPs on the two fronts have not been fully considered when using DS for practical applications, such as, pulse duration compression, amplification, pump-probing, supercontinuum generation.

A more general problem that been frequently encountered is the DS deterioration when the cavity gain is larger enough. In our case, pump

power beyond 70 mW, whose optical spectrum is shown in Fig. 2 (d). Its corresponding SOP information on the Poincaré sphere and in the phase diagram are depicted in Figs. 4(g)-(j). During the soliton explosion, it is clear that more frequencies with freak or rogue positions in the phase diagram have been observed when the DS is deteriorated by larger cavity gain. Besides, the probability for generating such a kind of freak frequencies seems to increasing with the gain. This trend is obvious when comparing the single-shot spectra in Figs. 3 (c) and 3 (d), where the new frequencies on the two fronts are generated with unexpected high intensities. During the dissipative soliton explosion, the system cannot be self-sustaining. Also, those new frequencies are fundamentally different from those when cavity gain is insufficient. For example, fundamental order of quasi-DSs are frequently encountered for pump power at 45 mW, while no freak SOP distribution has been observed for the whole lasing spectrum.

To quantitatively characterize the SOP distributions in the buildup of DS, we give a dimensionless parameter, r , describing the relative distance between arbitrary two points of two Stokes vectors.

$$r = \sum_{\substack{m,n=1 \\ m \neq n}}^N |\hat{S}_m - \hat{S}_n| = \sum_{\substack{m,n=1 \\ m \neq n}}^N \sqrt{(s_{m1} - s_{n1})^2 + (s_{m2} - s_{n2})^2 + (s_{m3} - s_{n3})^2} \quad (2)$$

We calculate the averaged value of r for different cavity gains. Figure 5 plot the r_{ave} for various filtered wavelengths in the half blue part of the spectrum (The cures in the red half part are not show as they are symmetric to those in the blue half part). It is obviously that the relative distance of a specific wavelength convergences exponentially into a fixed point with the increment of cavity gain. The wavelength far away from the center region features a slower convergence rate.

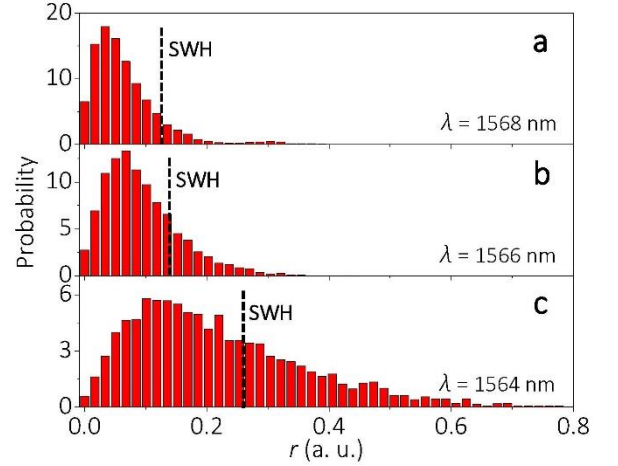


Fig. 6. Histograms for the relative distance between each point on the Poincaré spheres for pump power at 70 mW, when soliton explosion deteriorates the high coherence of DS. Large deviation from Gaussian distribution indicates the optical polarization rogue waves, which can also be certified by the SWH.

Further, we give the probability distribution function of r when the DS is deteriorated. As seen in Fig. 5, the quasi-Gauss shape distribution for wavelength at 1568 nm (the center region) is originated from the DS, although may be disturbed. Howbeit, for wavelengths far away from the center, a deviating trend to L-shaped probability distributions characters the emergences of extreme events in the polarization domain rather than in time or frequency domains [19,27-31]. This irregular polarization state of deteriorated DS is associated with the emergence of a new kind of optical rogue waves in the polarization domain, namely optical polarization rogue waves [13]. Just from the point of measurement in the phase histogram in Figs. 4 (i) and (j), those rogue events appear both with unexpected positions and probabilities [19]. From the statistical point of view, those polarization rogue waves can also be verified by the strong heavy tail in the measured histogram. We give the significant wave height (SWH) in Fig. 6, which is defined as

the mean amplitude of the highest third of the waves. As shown, 1.8 % of the events have the value larger than the twice of the SWH for wavelength at 1568 nm, while the rogue part could be 3.8 % for wavelength at 1564nm, and it is reasoning to anticipate that this rogue probability could be even larger when the cavity gain is further increasing.

4. CONCLUSION

We experimentally investigated the polarization evolution dynamics of DS fiber laser mode-locked by single-wall carbon nanotubes. When the cavity gain is increasing, the lasing system operates from random amplified spontaneous emission to stable DS, and the SOPs convergence exponentially into a fixed point. By introducing the phase diagram of the ellipticity angle and spherical orientation angle, we find that the SOP of each wavelength in the central region of the DS is linearly spaced, while those in the two fronts are spatially varying. Further enlarge the gain leading to optical spectrum broadening, and the new generated SOPs extend to scattering. Further increasing the pump power results into DS deterioration, and behave as soliton explosion. We identified a kind of polarization optical rogue waves by the strong heavy tail in the measured histogram through SWH method. Those experimental results provide more information for deeper insights into the transient dynamics of DS fiber laser, which can be of great interest for theory modelling, amplification, pump-probing, supercontinuum generation, et al. The related works on polarization rogue waves also provide a new insight into the still debated topic of the mechanisms for rogue waves.

Acknowledgment. This work was supported by the Natural Science Foundation of China (61635004, 61405023), the National Postdoctoral Program for Innovative Talents (BX201600200), the Postdoctoral Science Foundation of China (2017M610589), the Postdoctoral Science Foundation of Chongqing (Xm2017047), the Science Foundation of Chongqing (CSTC2017JCYA0651), and the Fundamental Research Funds for the Central Universities (106112017CDJXY120004). Stefan Wabnitz acknowledges support by the Italian Ministry of University and Research (MIUR) (2015KEZNYM), the Horizon 2020 MSCA-RISE 2015 project CARDIALLY, and the Russian Ministry of Science and Education (14.Y26.31.0017).

REFERENCES

1. P. Grelu and N. Akhmediev, "Dissipative solitons for mode-locked lasers," *Nat. Photon.* **6**, 84–92 (2012).
2. J. M. Dudley, F. Dias, M. Erkintalo, G. Genty, "Instabilities, breathers and rogue waves in optics," *Nature Photon.* **220**, 755-764 (2014).
3. C. Lecaplain, P. Grelu, J. M. Soto-Crespo, N. Akhmediev, "Dissipative rogue waves generated by chaotic pulse bunching in a mode-locked laser," *Phys. Rev. Lett.* **108**, 233901 (2012).
4. W. H. Renninger, A. Chong, and F. W. Wise, "Dissipative solitons in normal-dispersion fiber lasers," *Phys. Rev. A* **77**(2), 023814 (2008).
5. N. Akhmediev and A. Ankiewicz, eds., *Dissipative Solitons* (Springer, 2005).
6. K. Goda and B. Jalali, "Dispersive Fourier transformation for fast continuous single-shot measurements," *Nat. Photon.* **7**(2), 102–112 (2013).
7. G. Herink, B. Jalali, C. Ropers, and D. R. Solli, "Resolving the build-up of femtosecond mode-locking with single-shot spectroscopy at 90 MHz frame rate," *Nature Photon.* **10**, 321-326 (2016).
8. H. J. Chen, M. Liu, J. Yao, S. Hu, J. B. He, A. P. Luo, W. C. Xu, and Z. C. Luo, "Buildup dynamics of dissipative soliton in an ultrafast fiber laser with net-normal dispersion," *Opt. Express* **26**(3), 2972–2982 (2018).
9. K. Krupa, K. Nithyanandan, and P. Grelu, "Vector dynamics of incoherent dissipative optical solitons," *Optica* **4**(10), 1239-1244 (2017).
10. Z. Liu, S. Zhang, F. W. Wise, "Rogue waves in a normal-dispersion fiber laser," *Opt. Lett.* **40**, 1366-1369 (2015).
11. L. Gao, T. Zhu, S. Wabnitz, M. Liu, and W. Huang, "Coherence loss of partially mode-locked fiber laser," *Sci. Rep.* **6**, 24995 (2016).

12. D. V. Churkin, S. Sugavanam, N. Tarasov, S. Khorev, S.V. Smirnov, et al, "Stochasticity, periodicity and localized light structures in partially mode-locked fiber lasers," *Nature Commun.* **65**, 700 (2015).
13. L. Gao, T. Zhu, S. Wabnitz, Y. Li, X. S. Tang, and Y. Long Cao, "Optical puff mediated laminar-turbulent polarization transition," *Opt. Express.* **26**(5), 6103-6113 (2018).
14. T. Godin, B. Wetzel, T. Sylvestre, L. Larger, A. Kudlinski, A. Mussot, A. B. Salem, M. Zghal, G. Genty, F. Dias, and J. M. Dudley, "Real time noise and wavelength correlations in octave-spanning supercontinuum generation," *Opt. Express.* **21**(5), 18452-18460 (2013).
15. P. Suret, R. E. Koussaifi, A. Tikan, C. Evain, S. Randoux, C. Szwaj, and S. Bielawski, "Single-shot observation of optical rogue waves in integrable turbulence using time microscopy," *Nature Commun.* **7**:13136 (2016).
16. P. Ryczkowski, M. Närhi, C. Billet, J. M. Merolla, G. Genty, and J. M. Dudley, "Real-time full-field characterization of transient dissipative soliton dynamics in a mode-locked laser," *Nature Photon.* **12**, 221–227 (2018).
17. S. V. Sergeev, C. Mou, E. G. Turitsyna, A. Rozhin, S. K. Turitsyn, "Spiral attractor created by vector solitons," *Light Science & Applications* **3**, e131 (2014).
18. D. Li, D. Shen, L. Li, D. Tang, L. Su, and L. Zhao, "Internal polarization dynamics of vector dissipative-soliton-resonance pulses in normal dispersion fiber lasers," *Opt. Lett.* **43**(6), 1222-1225 (2018).
19. D. R. Solli, C. Ropers, P. Koonath, B. Jalali, "Optical rogue waves," *Nature* **450**, 1054-1057 (2007).
20. E. G. Turitsyna, S. V. Smirnov, S. Sugavanam, N. Tarasov, X. Shu, S. A. Babin, E. V. Podivilov, D. V. Churkin, G. Falkovich, and S. K. Turitsyn, "The laminar-turbulent transition in a fiber laser," *Nat. Photon.* **7**(10), 783–786 (2013).
21. V. Kalashnikov, S. V. Sergeev, G. Jacobsen, S. Popov, S. K. Turitsyn, "Multi-scale polarisation phenomena," *Light Science & Applications* **5**, e16011 (2016).
22. C. Mou, S. V. Sergeev, A. G. Rozhin, and S. K. Turitsyn, "Bound state vector solitons with locked and precessing states of polarization," *Opt. Express.* **21**(22), 26868-26875 (2013).
23. Y. J. Li, L. Gao, T. Zhu, Y. L. Cao, M. Liu, D. R. Qu, F. Qiu, and X. B. Huang, "Graphene-assisted all-fiber optical-controllable laser," *IEEE J. Sel. Top. Quant.* **24**(3), 1-9 (2018).
24. L. Gao, T. Zhu, W. Huang, and Z. Luo, "Stable, ultrafast pulse mode-locked by topological insulator Bi₂Se₃ nanosheets interacting with photonic crystal fiber: from anomalous dispersion to normal dispersion," *IEEE Photon. J.* **7**(1), 3300108 (2015).
25. A. F. J. Runge, N. G. R. Broderick, and M. Erkintalo, "Observation of soliton explosions in a passively mode-locked fiber laser," *Optica* **2**(1), 36-39 (2015).
26. W. Chang, A. Ankiewicz, J. M. Soto-Crespo, and N. Akhmediev, "Dissipative soliton resonances," *Phys. Rev. A* **78**, 023830 (2008).
27. K. Hammani, B. Kibler, C. Finot, A. Picozzi, "Emergence of rogue waves from optical turbulence," *Phys. Lett. A* **374**, 3585-3589 (2010).
28. D. R. Solli, G. Herink, B. Jalali, C. Ropers, "Fluctuations and correlations in modulation instability," *Nature Photon.* **6**, 463-468 (2012).
29. M. Onorato, S. Residori, U. Bortolozzo, A. Montina, F. T. Arecchi, "Rogue waves and their generating mechanisms in different physical contexts," *Phys. Rep.* **528**, 47-89 (2013).
30. J. P. Eckmann, "Roads to turbulence in dissipative dynamical systems," *Rev. Mod. Phys.* **53**, 643-654 (1981).
31. A. Picozzi, J. Garnier, T. Hansson, P. Suret, G. Randoux, et al, "Optical wave turbulence: Towards a unified nonequilibrium thermodynamic formulation of statistical nonlinear optics," *Phys. Rep.* **542**, 1-132 (2014).
32. S. A. Kolpakov, H. Khashi, and S. V. Sergeev, "Dynamics of vector rogue waves in a fiber laser with a ring cavity," *Optica* **3** (8):870-875 (2016).